Jun 27th, 10:40 AM - 12:00 PM

Spatio temporal analysis of floods at a catchment scale

Ignacio Fuentes
The University of Sydney, ignacio.fuentes@sydney.edu.au

Jose Padarian
University of Sydney, Australia, jose.padarian@sydney.edu.au

R.W. Vervoort
The University of Sydney, willem.vervoort@sydney.edu.au

iEMSs International Congress on Environmental Modelling and Software

9th International Congress on Environmental Modelling and Software

Fort Collins, Colorado, USA, Mazdak Arabi, Olaf David, Jack Carlson, Daniel P. Ames (Eds.)

https://scholarsarchive.byu.edu/iemssconference/2018/

Comparing Volume Estimates from Flood Detection Algorithms for Spatio-Temporal Analysis of Floods

Ignacio Fuentes[a]*, José Padarian[a], R. Willem Vervoort[a]

[a]School of Life and environmental Sciences, The University of Sydney, New South Wales, Australia
ignacio.fuentes@sydney.edu.au

ABSTRACT

Episodic flood events have a significant impact on ecosystems and human settlements, and can be important drivers for the water availability. This study maps the flood extension at a catchment scale, and determines the volumes associated with inundation events for selected return periods by coupling a water detection algorithm and three methods for water depth estimation. The study was carried out in the Namoi catchment of Australia by using the Google Earth Engine platform. The extension of inundated areas was obtained by applying the open water likelihood (OWL) algorithm on MODIS surface reflectance imagery. For the estimation of the associated water volumes, three different data driven methodologies were compared, all of which use digital elevation models (DEM) to obtain water depths. These involve the obtaining of the maximum elevation in the flooded polygons, and the use of the Cohen and Doble algorithms. Two DEM products were used, a 5 m resolution LiDAR dataset of the floodplain in the catchment and the 1 second SRTM derived elevation model. Flood volumes were compared with rainfall volumes and the discharge at several gauge stations located at different reaches of the river. Return periods were obtained from the probabilities of pixels being inundated in a year. The relation between flood volume estimations and the stream discharge varied depending on the gauge position in the catchment. Flood volume estimation was improved using methods that took into account the flood pattern connection with the channels. A single flood frequency curve was developed for the entire catchment.

Keywords: Flood Mapping; Water Volumes; Remote Sensing; Google Earth Engine.

1. INTRODUCTION

Globally unsustainable production and exploitation rates create significant uncertainty about the future of the planet (Schewe et al., 2014). Quantifying water resources to assist water management plans or risk assessments therefore remains a priority (Poff et al., 2016)

Remote sensing use in estimating water resources has been increasing (Mueller et al., 2016), and can be applied together with direct measurements to assess the state and temporal variation of processes (Doble et al., 2016; Siev et al., 2016). The advantage of satellite imagery, relative to many other data sources is its ability to capture spatial variability of features at the surface (Mueller et al., 2016). While gauge and meteorological stations collect data at specific locations (Alsdorf et al., 2007), satellites cover a large spatial area (Gupta, 2018). On the other hand, satellites also measure the same spot at different times, which gives a time series (Siev et al., 2016). There are several satellites with different resolutions, capturing different wavelength ranges (Gupta, 2018; Schmugge et al., 2002). In addition, not all satellites have operated over the same timeframe, with some of the more detailed spatial products being relatively recent (Sentinel; Nagler et al. 2015)

While water detection from space captures the spatial extent of water on the surface, it does not necessarily provide water quantities in flood events (Zhou et al., 2017). As a result, data driven methods have been developed to estimate inundation volumes by coupling flood extension imagery with gauge station measurements, bathymetry or digital elevation models (DEM; Cohen et al., 2017; Doble et al., 2014; Siev et al., 2016). Several approaches have been tested, but the performance against field measurements has mostly been through spatial snapshots rather than studying the

temporal dynamics (Cohen et al., 2017), or have been studied mostly in the short term (Frappart et al., 2005; Siev et al., 2016)
The tendency for short period flood studies, using remote sensing, is mainly caused by difficulties of acquiring large amounts of remote sensing information and related preprocessing (Ma et al., 2015). However, an important innovation has been the development of the Google Earth Engine platform, which contains multi-petabyte processed geospatial datasets that are being updated and uploaded constantly (Gorelick et al., 2017).
The second main difficulty to assess inundation volumes is the lack of a reference to compare the results (Oreskes et al., 1994). Most of the time, information from gauge stations, dams, or the inputs of water to the system, such as rainfall, are used, all of which allow a rough water availability estimation (Alsdorf et al., 2007). However, more alternatives have been developed in the last years, such as the use of gravity satellite imagery (GRACE), and in the next years the launch and operation of the Surface Water and Ocean Topography mission (SWOT) is expected to produce more accurate estimations of surface water in the future (Fu and Ubelmann, 2014).
The main objective of this study was to compare three different existing methodologies for water volume estimation with a water detection algorithm through Google Earth Engine to study long-term flood volume dynamics at the catchment scale.

2. MATERIALS AND METHODS

2.1. Study catchment

The selected 42,000 km^2 catchment is the Namoi, located in the north of NSW, Australia, formed by the Namoi river flowing westward. It has several major dams, storing water and regulating flow downstream. Another main hydrological characteristic are on-farm “ring tank” dams for irrigation, which can be up to 100 ha.
The yearly mean precipitation in the catchment is 800 mm, whilst the mean annual potential evapotranspiration is around 1300 mm (McCallum et al., 2010). Floods in the Namoi catchment are periodic natural events with a significative environmental role for local wetlands (Green et al., 2011), but also causing potential economical and humanitarian losses. The catchment elevation ranges from 125 m.a.s.l., in the west, and increases eastwards up to 1,501 m.a.s.l. This height gradient is one of the main factors that influences areas prone to inundation in the catchment.

2.2. Data selection

Data from several gauging stations in the catchment was used in this study. Daily stream levels and discharges are freely available at the waterinfo webpage, from the New South Wales government (http://waterinfo.nsw.gov.au/). Daily rainfall grids at a resolution of 0.05 degrees were obtained from the Bureau of Meteorology of the Australian Government (http://www.bom.gov.au). The grids were clipped at the extension of the basin and rainfall was daily summed to estimate the total volume of water entering the catchment. Satellite imagery used were the daily and the 8 days composite surface reflectance datasets obtained from the MODIS Terra satellite (MOD09GA and MOD09A1, respectively) from 2000 to 2018. These datasets, available in the Google Earth Engine platform, were preprocessed removing clouds, shadows, and smoke from fires, and subsequently masked in order to remove pixels that were affecting the detection of water at the margin of tiles and in the range of the shortwave infrared wavelength. Additionally, permanent water bodies were masked using the Land Water Mask Derived from MODIS and SRTM (MOD44W). A SRTM Derived Hydrological Elevation Model at 1 arcsec resolution and a 5 m Digital Elevation Model (DEM) of Australia derived from LiDAR, both available in the Google Earth engine platform, were used to obtain the water depths in flooded areas, and to derive a multiresolution index of valley bottom flatness (MrVBF) map of the catchment. Both DEMs were used and compared, but the LiDAR DEM does not comprise the entire catchment, but only an area that covers some of the floodplains. In spite of this, the vertical resolution of this DEM is significantly more accurate than that from the SRTM DEM, which does cover the entire extension of the catchment.

2.3. Inundation estimations

In order to estimate the flood extent, the Open Water Likelihood (OWL) algorithm (Guerschman et al. 2011) was used, which gives the probability of finding water in each pixel. The MrVBF used as input in the algorithm was derived from the SRTM DEM, and a threshold of 0.87 was applied to the OWL data to select inundated areas because this value gave the best estimates of actual flood extent (results not shown).
To estimate the water volumes from the flood extension data obtained, three methods that use DEMs or bathymetric images were utilised, allowing to get the depth of water at surface, which was subsequently multiplied by the inundation areas at each pixel. For all methods, the inundation area was constrained to the area covered by the LiDAR imagery in order to compare the results using both, the SRTM and the LiDAR DEMs. The water depth estimation methods used are described below:

- The first method assumes that the water surface during floods is flat (Siev et al., 2016). Polygons of inundated areas are obtained and overlain by the DEM, and the maximum elevation of water in the perimeter of polygons is assumed to be the surface water elevation. Then, the DEM is subtracted to get the water depth.
- In the second method the DEM was converted into an array of 100 matrices by obtaining the percentiles of all DEM pixels (30 m resolution) included in each MODIS pixel (500 m resolution). Then, an elevation image was created by selecting the elevation percentile of the array in each pixel corresponding to the probability estimated by the OWL algorithm. The original DEM was subsequently subtracted from these elevations to obtain the water depth at each pixel (Doble et al., 2014). All negative values calculated were converted to 0, and only areas with an OWL threshold of 0.87 were classified as inundated.
- The last method was developed by Cohen et al. (2017). It involves a conversion of inundated areas into polygons to obtain the elevations at the perimeter of polygons, and subsequently it applies a focal mean in a series of iterations to populate the area inside the polygons with water elevations. The final stage implies subtracting the water elevations from the original DEM to get the water depths. Negative water depths are converted to 0, and a final focal mean with a kernel of 3 pixels is carried out to smooth any abrupt change on the water elevations.

2.4. Occurrence probability and statistical analysis

Using the flooded areas from the OWL algorithm probability maps were calculated out in Google Earth Engine. For each year, the maximum inundated area was estimated. Then, the probability of inundated pixels was obtained using Kuczera and Franks (2016):

$$P_{i,j} = \frac{m - 0.4}{n + 0.2}$$

where $P_{i,j}$ is the occurrence probability for each pixel, being *i* and *j* the pixel positions in the image, *m* corresponds to number of occurrences and *n* to the number of years on record. Then, the return period is calculated as the inverse of the probability of occurrences. From the occurrence probability maps an estimate of inundated volumes was calculated, which gave flood frequency curves at a catchment scale. These curves were compared with flood frequency curves estimated from gauge stations using the same methodology.

3. RESULTS AND DISCUSSION

The algorithms result in different inundation volumes (Figure 1). In general, the algorithm that takes into account the maximum water levels, predicts inundation values that are around two orders of magnitude greater than the Cohen algorithm, and at least one order of magnitude higher than using the OWL probabilities (Doble et al, 2014).

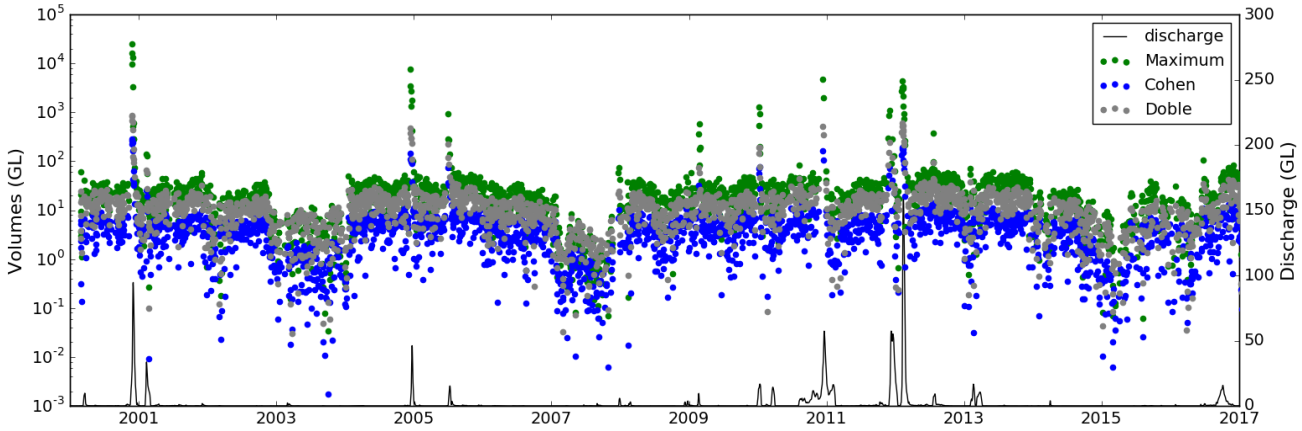

Figure 1. Time series of inundation volumes estimated and daily discharges at Walgett.

All the inundated volume time series capture the peak of discharges in the stream, and also present a seasonal behaviour. The logarithmic scale allows to detect not just flood events, but also some periods where there is limited surface water, probably associated to drought periods, which can be observed in 2003, 2007 and 2015. In order to analyze how inundation volumes respond to rainfall, a cross correlation was carried out (Figure 2).

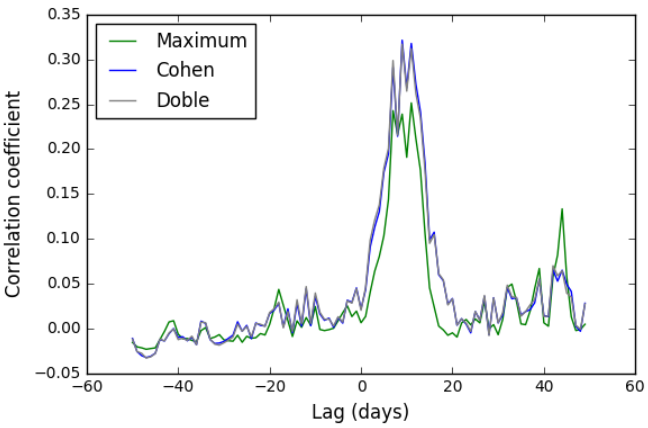

Figure 2. Cross correlation between inundated volumes and daily rainfall.

As it is expected, there is a delay in the response of floods to rain, with the highest correlations found after 10 days. In this case, the Cohen and Doble algorithms have very similar correlations, which are in general higher than those obtained using the maximum DEM values.
Taken into account the lagged response observed, a scatter plot between monthly accumulated rainfall and monthly accumulated inundated volumes can be assessed for each methodology (Figure 3). Accumulated volumes should be expected to be always lower than accumulated rainfall, considering that rain corresponds to the input of water to the system and that surface waters are just a fraction of the available water of the system.

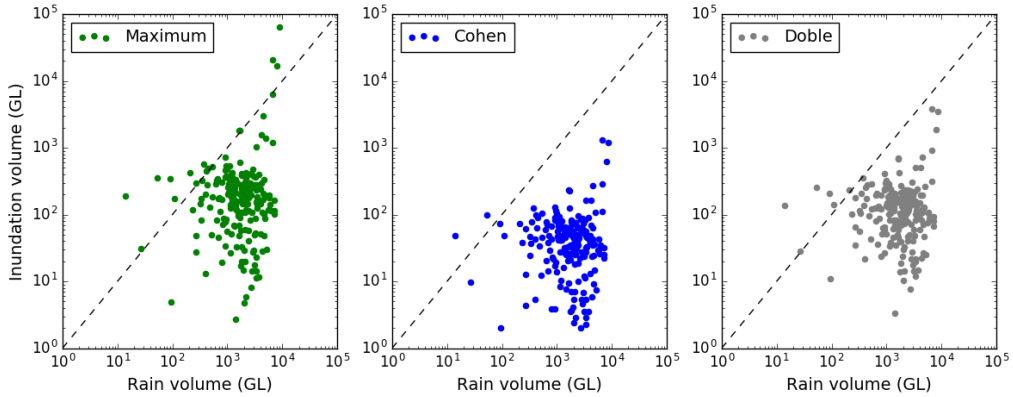

Figure 3. Scatterplots of monthly accumulated rainfall and monthly accumulated inundation volumes.

In the case of the maximum elevation methodology used, some accumulated inundation volumes are significantly higher than accumulated rainfall. This was also tested by assessing the maximum and

minimum values of the perimeter of inundation polygons. In most cases, and for small inundation polygons, the difference between the minimum and maximum elevation values was not significant (lower than 0.5 m). However, during flood events, big inundation polygons surrounding the main stream could be observed, and the perimeter had elevations ranging in some cases higher than 10 m, which means that this methodology fails to meet the original assumption of flat water surfaces, and implying that part of the inundation volumes detected is still flowing through the main streams (Frappart et al., 2005).
The relationship between the inundated volumes and the daily discharges in the stream gauges of he Namoi river at Bugilbone and Walgett (both in the lower western part of the catchment, Figure 4) indicates a fairly linear relationship with correlation coefficients ranging from 0.57 to 0.93, depending on the methodology. The lowest correlation is for the maximum elevation methodology, whilst the other two methods have quite similar correlation coefficients.

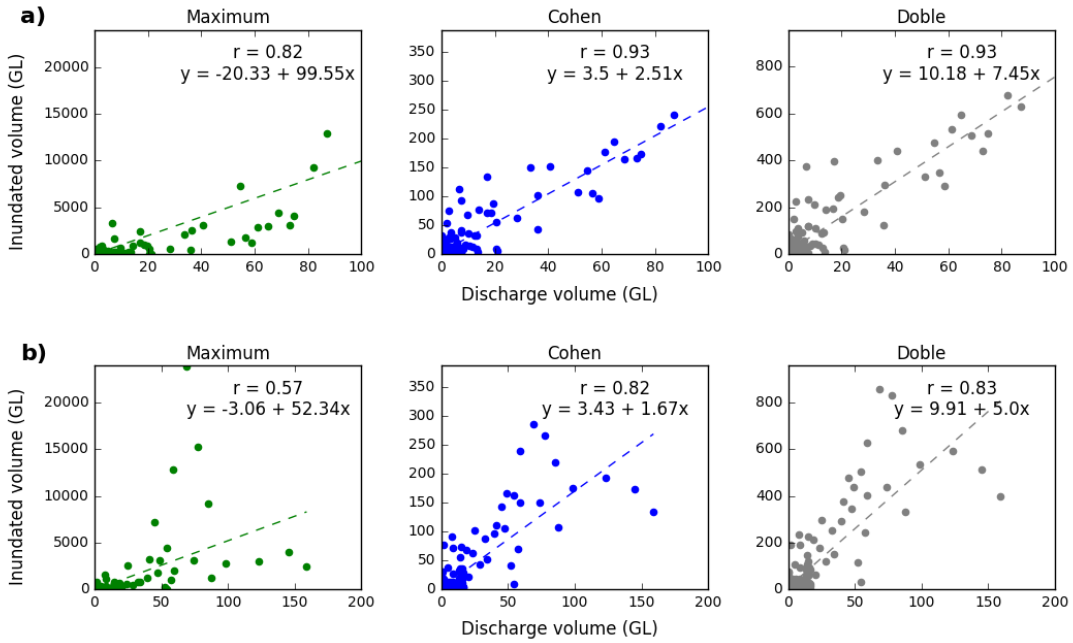

Figure 4. Scatterplots of inundated volumes against daily discharge volumes in the Namoi river at Bugilbone (above) and Walgett gauge stations (below).

A cross correlation between daily discharge at all stations in the catchment and daily flood volumes in the LiDAR DEM locations identified the maximum cross correlation coefficients (left below, Figure 5) and associated time lag between the flood volume and occurence of discharge (left above, Figure 5). Is it clear that in the lower (western) part of the catchment, lags are smaller and even positive (indicating the flooding occurs before the gauge registers an increase in flow). These areas which receive all the upstream flow, also have higher correlation values than the gauges located in the east of the catchment (higher elevations). The eastern (upstream) part of the catchment, also indicates stronger negative lags, meaning the flooding follows the increase in flow at the gauge.
Different locations in the catchment have different lags between rainfall and flooding, which can assist with forecasting, but also gives information about the rate of surface water movement in the catchment (Alsdorf et al., 2007).

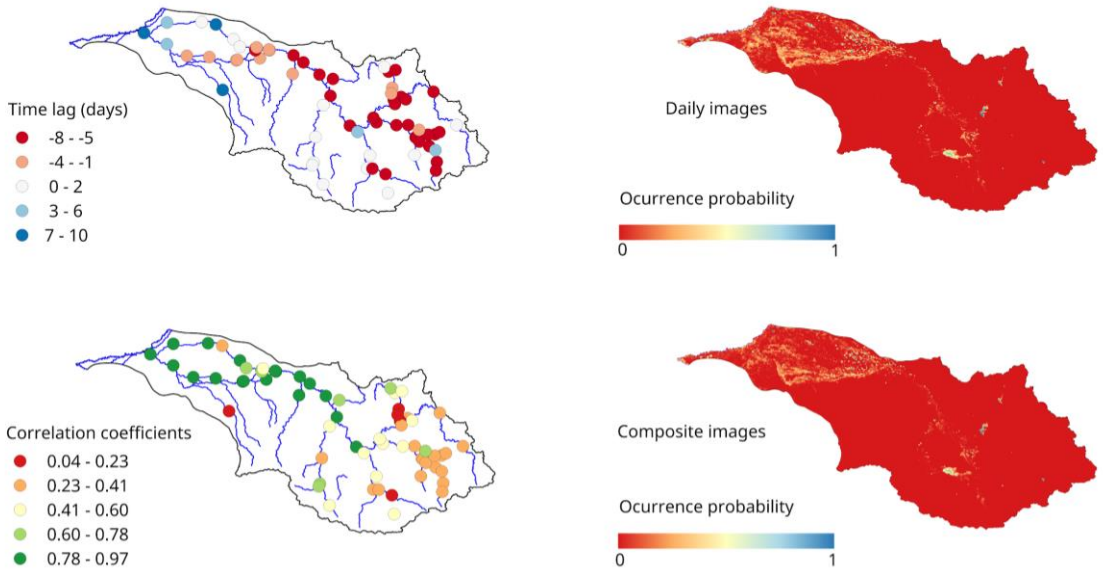

Figure 5. Maximum cross correlation coefficients between daily discharge at different locations in the catchment and inundation volumes (left below) obtained within different time lags (left above), and occurrence probability maps using daily (MOD09GA; right above) and 8 days composite (MOD09A1; right below) imagery.

The deviation of linear regression slopes, obtained between daily discharge and inundation volumes with the different time lags used above, from a 1:1 line can be used to estimate the proportion of water losses other than stream discharge (evapotranspiration and recharge). This varies by reach of the river, and the distance to the flood sinks (Figure 6).

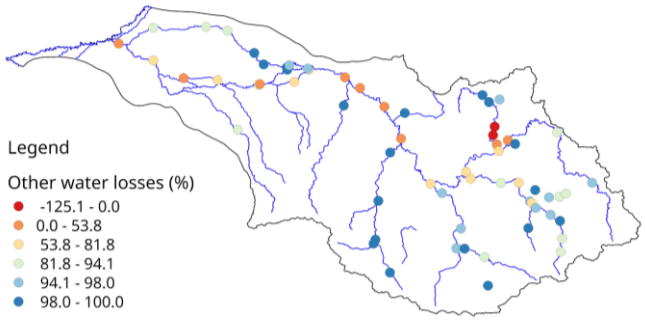

Figure 6. Proportion of water losses other than stream discharge obtained through the deviation of regression slopes from a 1:1 line.

Thus, whilst in the main reach of the Namoi river from Boggabri downstream a fairly even proportion of water losses occurs, Pian Creek and elevated sectors of the catchment have a much higher proportion of losses by recharge and evapotranspiration, with some locations near Wee Waa showing very high water loss. In this area, it has been identified a significant surface-groundwater interaction (Kelly et al., 2009), which is recharging the Namoi aquifer, and would shift the slope of the regressions. Negative fractions are observed at two gauges, which also have the lowest correlation coefficients between flood and discharges in the catchment. These are located immediately downstream the Chaffey dam, one of the major water reservoirs in the basin, which also regulates the flow downstream (Green et al., 2011).

Occurrence probability images obtained from the OWL algorithm by using daily and composite imagery (Figure 5) were processed to estimate the frequency of flood events in the catchment and compared with flood frequency curves obtained from the Namoi river at Walgett and Bugilbone gauging stations (Kuczera and Franks, 2016; Figure 7). Flood frequency curves from the Cohen and the Doble algorithms are significantly different, being much lower for the Cohen methodology, especially at small return periods. Additionally, whilst in the Cohen methodology the use of the LiDAR DEM always leads to smaller inundation volumes, in the Doble methodology the flood frequency curves overlap, and the difference between the curves is smaller. The inundation volumes for the entire catchment (Cohen basin and Doble basin in Figure 7a) are significantly higher than those obtained for the extension covered by the LiDAR images, but follow the same general trend. The flood frequency curves from the river at Walgett and Bugilbone indicate similar behaviour (Figure 7b).

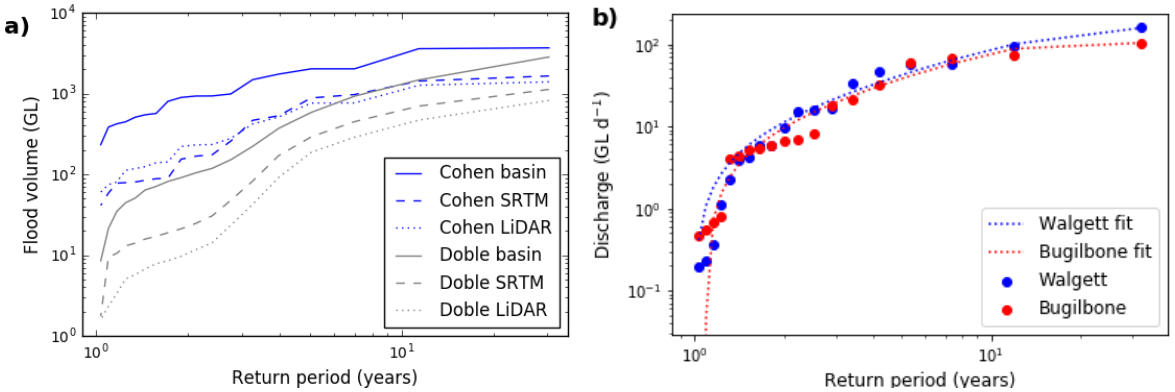

Figure 7. Flood frequency curves obtained from the temporal analysis of floof volume estimations (left), and from daily discharges in the Namoi river at Bugilbone and at Walgett (right).

4. CONCLUSIONS

A surface water detection algorithm and three water depth methodologies were coupled in order to get time series of inundation volume estimations at a catchment scale. The estimated volumes for all methods presented seasonal variation and captured peak discharge events. However, the method that assumes the maximum elevation of flooded polygons proved to be the worst as the water elevation of them demonstrated not to meet the assumption of a flat surface, and therefore overpredicts inundated volumes at big flood events. The other methodologies, despite differences in volume estimates, did not show significant differences in temporal behaviour. Rainfall is related to flooded volumes, but this relationship is higher several days after rainfall events. The relationship between inundation volumes and discharges at different locations in the catchment varies depending on the location. In general, downstream stations presented higher correlations and also a delay in the flow response to floods, whilst upstream stations presented lower correlation coefficients and its discharge peaks precedes the flood occurrence. In addition, the slope of the linear regression between daily discharges and daily inundation volumes and its deviation from a 1:1 line, which can allow to obtain the proportion of other water losses, such as recharge or evapotranspiration, also changes according to the position in the catchment, and especially depending on the reach where the stations are located, which means that the distance to flood sinks, and hydraulic properties of the sediments are affecting the flood-discharge response. From water occurrence probability maps, flood frequency curves were obtained for the entire catchment, presenting a behavior similar to curves calculated from gauge stations. The results obtained can help to the understanding of the hydrological cycle and the processes related, and also to define management plans and hydraulic design thresholds.

ACKNOWLEDGEMENTS

The first author was supported through a scholarship by the Chilean Government (“Becas Chile”, Comisión Nacional de Investigación Científica y Tecnológica, CONICYT).

REFERENCES

Alsdorf, D.E., Rodríguez, E., Lettenmaier, D.P., 2007. Measuring surface water from space. Reviews of Geophysics 45. https://doi.org/10.1029/2006RG000197

Cohen, S., Brakenridge, G.R., Kettner, A., Bates, B., Nelson, J., McDonald, R., Huang, Y., Munasinghe, D., Zhang, J., 2017. Estimating floodwater depths from flood inundation maps and topography. Journal of the American Water Resources Association (JAWRA) 1-12. https://doi.org/10.1111/1752-1688.12609

Doble, R., Crosbie, R., Peeters, L., Joehnk, K., Ticehurst, C., 2014. Modelling overbank flood recharge at a continental scale. Hydrology and Earth System Sciences 18, 1273–1288. https://doi.org/10.5194/hess-18-1273-2014

Frappart, F., Seyler, F., Martinez, J.-M., León, J.G., Cazenave, A., 2005. Floodplain water storage in the Negro River basin estimated from microwave remote sensing of inundation area and water levels. Remote Sensing of Environment 99, 387–399. https://doi.org/10.1016/j.rse.2005.08.016

Fu, L.-L., Ubelmann, C., 2014. On the Transition from Profile Altimeter to Swath Altimeter for Observing Global Ocean Surface Topography. Journal of Atmospheric and Oceanic Technology 31, 560–568. https://doi.org/10.1175/JTECH-D-13-00109.1

Green, D., Petrovic, J., Moss, P., Burrell, M., 2011. Water resources and management overview: Namoi catchment, NSW Office of Water, Sydney, 31 p.

Gorelick, N., Hancher, M., Dixon, M., Ilyushchenko, S., Thau, D., Moore, R., 2017. Google Earth Engine: Planetary-scale geospatial analysis for everyone. Remote Sensing of Environment 202, 18–27. https://doi.org/10.1016/j.rse.2017.06.031

Guerschman, J.P., Warren, G., Byrne, G., Lymburner, L., Mueller, N., Van-Dijk, A., 2011. MODIS-based standing water detection for flood and large reservoir mapping: algorithm development and applications for the Australian continent. Water for a Healthy Country National Research Flagship Report, Canberra.

Gupta, R.P., 2018. remote sensing geology, 3rd Edition. Springer-Verlag, Berlin.

Kelly, B.F.J., Allen, D., Ye, K., Dahlin, T., 2009. Continuous electrical imaging for mapping aquifer recharge along reaches of the Namoi River in Australia. Near Surface Geophysics 7, 259–270.

Kuczera, G., Franks, S., 2016. At-site flood frequency analysis, Book 3 in Australian Rainfall and Runoff - A Guide to Flood Estimation, Commonwealth of Australia.

Ma, Y., Wu, H., Wang, L., Huang, B., Ranjan, R., Zomaya, A., Jie, W., 2015. Remote sensing big data computing: Challenges and opportunities. Future Generation Computer Systems 51, 47–60. https://doi.org/10.1016/j.future.2014.10.029

McCallum, J.L., Crosbie, R.S., Walker, G.R., Dawes, W.R., 2010. Impacts of climate change on groundwater in Australia: a sensitivity analysis of recharge. Hydrogeology Journal 18, 1625–1638. https://doi.org/10.1007/s10040-010-0624-y

Mueller, N., Lewis, A., Roberts, D., Ring, S., Melrose, R., Sixsmith, J., Lymburner, L., McIntyre, A., Tan, P., Curnow, S., Ip, A., 2016. Water observations from space: Mapping surface water from 25 years of Landsat imagery across Australia. Remote Sensing of Environment 174, 341–352. doi:10.1016/j.rse.2015.11.003

Nagler, T., Rott, H., Hetzenecker, M., Wuite, J., Potin, P., 2015. The Sentinel-1 Mission: New Opportunities for Ice Sheet Observations. Remote Sensing 7, 9371–9389. https://doi.org/10.3390/rs70709371

Oreskes, N., Shrader-Frechette, K., Belitz, K., 1994. Verification, validation, and confirmation of numerical models in the Earth Sciences. Science 263, 641-646. https://doi.org/10.1126/science.263.5147.641

Poff, N.L., Brown, C.M., Grantham, T.E., Matthews, J.H., Palmer, M.A., Spence, C.M., Wilby, R.L., Haasnoot, M., Mendoza, G.F., Dominique, K.C., Baeza, A., 2016. Sustainable water management under future uncertainty with eco-engineering decision scaling. Nature Climate Change 6, 25–34. https://doi.org/10.1038/nclimate2765

Schewe, J., Heinke, J., Gerten, D., Haddeland, I., Arnell, N.W., Clark, D.B., Dankers, R., Eisner, S., Fekete, B.M., Colón-González, F.J., 2014. Multimodel assessment of water scarcity under climate change. Proceedings of the National Academy of Sciences 111, 3245–3250.

Schmugge, T.J., Kustas, W.P., Ritchie, J.C., Jackson, T.J., Rango, A., 2002. Remote sensing in hydrology. Advances in water resources 25, 1367–1385.

Siev, S., Paringit, E., Yoshimura, C., Hul, S., 2016. Seasonal Changes in the Inundation Area and Water Volume of the Tonle Sap River and Its Floodplain. Hydrology 3, 33. https://doi.org/10.3390/hydrology3040033

Zhou, Y., Dong, J., Xiao, X., Xiao, T., Yang, Z., Zhao, G., Zou, Z., Qin, Y., 2017. Open Surface Water Mapping Algorithms: A Comparison of Water-Related Spectral Indices and Sensors. Water 9, 256. doi:10.3390/w9040256